J. Fluid Mech. (1982), *vol.* 116, *pp.* 393–409
Printed in Great Britain

Equilibrium shape and stability of a liquid cylinder in cross flow at low Weber numbers

By D. WEIHS AND I. FRANKEL
Department of Aeronautical Engineering,
Technion-Israel Institute of Technology, Haifa, Israel

(Received 18 November 1980 and in revised form 8 August 1981)

The cross-section shape and stability of a liquid cylinder moving perpendicularly to its axis in a gaseous medium is studied. Such liquid cylinders are formed during the break-up process of thin, rapidly moving liquid sheets, appearing in spray and atomization processes. The equilibrium shape is affected mainly by two factors: the dynamic-pressure distribution in the gas flow and the surface tension on the liquid boundary. The former tends to distort the liquid cross-section into an oval shape while the latter tends to restore the circular cross-section.

A series expansion for the shape of the cylinder cross-section was determined by assuming incompressible potential flow, neglecting the effects of body forces and internal circulation in the liquid.

The stability analysis shows that in the range of low Weber numbers the cylinder break-up is due to the divergence of varicose perturbations. The wavenumber of the most rapidly growing perturbation, its rate of growth and the maximal wavenumber for which varicose instability occurs, are all found to decrease as the Weber number grows, owing to a pressure distribution caused by the varicose distortion, which tends to reduce these perturbations.

1. Introduction

Spray and atomization processes appear in a variety of fields, including painting, fire-fighting, combustion, agriculture and aerosol production, among others. A common technique for producing such sprays is by formation of thin, rapidly moving liquid sheets by injection of the liquid through certain nozzle types (fan spray etc.) or by collision of liquid jets. Under appropriate conditions these sheets disintegrate owing to aerodynamic instability, causing atomization and droplet formation.

According to the commonly accepted (Brodkey 1967) model of the disintegration process (Dombrowski & Johns 1963), a wavy perturbation of the sheet builds up, giving it the typical form of a 'waving flag' (see figure 1). The amplitude of this perturbation grows, and when it reaches a critical value the sheet is torn transversely into ligaments. These liquid ligaments quickly contract into cylindrical segments through the action of surface tension. The cylinders then continue moving broadside and undergo a varicose type of break-up process.

The first phase of the sheet break-up process has been extensively studied by Squire (1953), Hagerty & Shea (1955), Dombrowski and various coworkers (Dombrowski, Hasson & Ward 1960; Dombrowski & Hooper 1962; Fraser *et al.* 1962;

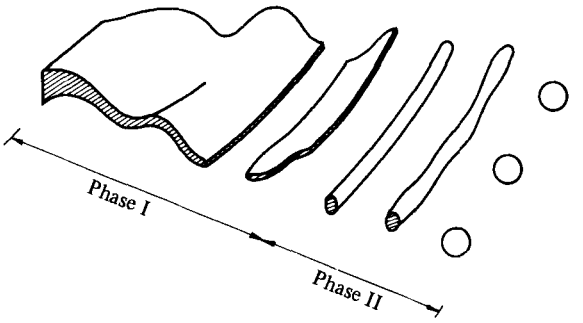

FIGURE 1. The Dombrowski & Johns (1963) model for liquid-sheet break-up and atomization.

Dombrowski & Johns 1963; Clark & Dombrowski 1972; Crapper, Dombrowski, Jepson & Pyott 1975; Crapper, Dombrowski & Pyott 1975), Weihs (1978), and others.

For the second phase of the disintegration process, i.e. from the formation of the cylinders to their break-up into drops, Rayleigh's classical solution for the break-up of a non-moving liquid cylinder under the action of surface tension has usually been adopted. (Fraser *et al.* 1962; Dombrowski & Hooper 1962; Dombrowski & Johns 1963; etc.). Thus, previous investigations have essentially ignored the effect of relative motion of the surrounding atmosphere on the stability of the liquid cylinder.

The stability of a liquid jet moving along its axis has been extensively investigated (Levich 1962; Sterling & Sleicher 1975; Anno 1977; Bogy 1979; and others). These studies modified and extended the classic solutions of Rayleigh (1894) and Weber (1931) to include nonlinear effects, inertia and viscosity of the liquid and gas, the influence of surfactants etc., and to cover a wider range of flow parameters (jet velocities etc.). However, the effect of cross flow on the jet has not been examined. This cross-flow effect, while appearing mainly in spray jets, can also occur when ink-jet nozzles (Bogy 1979) perform a sideways or rotating motion.

The purpose of the present paper is thus to study the equilibrium cross-section and stability of a liquid cylinder moving perpendicularly to its axis in a gaseous medium.

2. Formulation of the problem

The two main factors affecting the equilibrium shape of the cylinder cross-section are the dynamic-pressure distribution in the surrounding flowing gas and the surface tension on the gas–liquid boundary.

The pressure distribution tends to compress the cylinder in the direction of the motion and stretch it in the perpendicular direction. Thus the cross-section is distorted into an oblate shape (see figure 2). It is easily seen that the greater the distortion the more the pressure distribution tends to increase it.

On the other hand, the distortion just described changes the local curvature of the gas–liquid boundary in a manner which increases curvature and surface tension on the diameter perpendicular to the gas flow and decreases them on the diameter in the direction of the motion. Thus the surface tension acts to balance the dynamic-pressure effects.

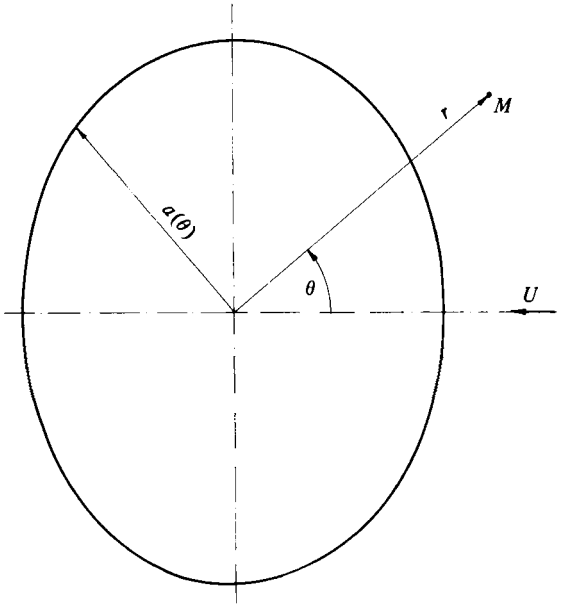

FIGURE 2. Schematic description of equilibrium cross-section shape of a liquid cylinder subjected to a cross flow of speed U, and the co-ordinate system. (The figure actually shows the calculated shape for $W = 0{\cdot}3$.)

The possible influence of several other factors have been omitted in order to facilitate the present solution.

(1) Taking cases where the flow Reynolds number $Re = 2\rho_g U a_0/\mu_g \gg 1$ where ρ_g is the gas density, μ_g the gas viscosity, U the flow velocity and a_0 the equivalent radius (the radius of a circular cylinder with the same cross-sectional area), because typical spray velocities are $O(10$ m/s) and cylinder diameters are up to $O(10^{-3}$ m), the influence of the shear stress on the gas–liquid boundary is neglected relative to the dynamic pressure. The flow is then taken to be potential.

As a result, flow separation and its possible effects on the pressure distribution are neglected. (For an approximate analysis of the effects of separation on the cross-section shape, see the appendix.)

(2) Internal circulation in the cylinder is neglected. While no experimental evidence for the flow in cylinders of the size mentioned above was found, spherical droplets of this size range under comparable conditions ($Re > 100$, $W < 0{\cdot}16$) have been shown experimentally and numerically (Pruppacher & Pitter 1971; LeClair *et al.* 1972) to have negligible internal circulation.

(3) The influence of gravitation on the pressure inside the liquid is negligible compared with the influence of surface tension provided that the Bond number

$$B = (\rho_l - \rho_g)\, a_0^2 g/\delta \ll 1,$$

where ρ_l is the liquid density, g is the gravitational acceleration and δ is the coefficient of surface tension. Experimental data for fan-spray jets (Dombrowski & Johns 1963; Tanasawa, Sasaki & Nagai 1957) indicate that $B = O(10^{-3})$.

(4) The velocities commonly encountered in the disintegration processes mentioned

in § 1 are usually of $M < 0{\cdot}1$, where M is the Mach number, so that the gas is assumed incompressible.

(5) The longitudinal curvature of the cylinder (figure 1) is neglected, as the radius of curvature is very much larger than the cylinder equivalent radius.

(6) Experimental evidence (Dombrowski & Johns 1963; etc.), as well as a calculation based on the accelerations due to surface tension causing the contraction of the broken sheet into a cylinder (figure 1), indicate that this contraction has a time scale of two orders of magnitude less than the break-up time. Thus the equilibrium shape can be viewed as a steady state, although it was rather violently formed. Any residual vibrations can also be seen as part of the perturbations that eventually cause instability and break-up of the cylinder.

3. Analysis of equilibrium shape

The equilibrium cross-section shape is thus assumed to be the result of the balance of surface tension and dynamic pressure distribution only, as a result of the previous simplifications. Therefore, the equilibrium condition for pressure at the interface is

$$p_a + \frac{\delta}{R} = E, \tag{1}$$

where p_a is the external pressure on the cylinder surface, R is the local radius of curvature of the gas–liquid interface and E is the pressure in the liquid. (As a result of neglecting body forces and internal circulation, we may conclude that the liquid pressure is uniform in the equilibrium state.)

We now look for the shape $r = a(\theta)$ for which the equilibrium condition (1) is fulfilled (r, θ are polar co-ordinates according to figure 2). In spite of the simplifications made so far, the solution of the problem in hand is still rather complicated, as the pressure distribution is coupled with the cylinder cross-section shape $a(\theta)$. Furthermore, the dependence of the pressure distribution on the velocity distribution (via Bernoulli's law) and the expression for the curvature are both nonlinear.

In order to overcome these difficulties we further limit ourselves to cases where the Weber number $W = \rho_g U^2 a_0/\delta \ll 1$, so that the equilibrium cross-section is described by slight deviations from the circular shape appearing when $W = 0$. The cylinder shape $a(\theta)$ and the velocity potential $\phi(r, \theta)$ of the gas flow can then be written as

$$a(\theta) = a_0[1 + Wf_1(\theta) + W^2 f_2(\theta) + \ldots], \tag{2}$$

$$\phi(r, \theta) = \phi_0(r, \theta) + W\phi_1(r, \theta) + W^2\phi_2(r, \theta) + \ldots, \tag{3}$$

where ϕ_0 is the velocity potential of the flow field exterior to a circular cylinder of radius a_0.

The pressure in the gas flow about the cylindrical surface is given from Bernoulli's law, to first order in ϕ, as

$$p_a(\theta) \simeq P_0 - \tfrac{1}{2}\rho_g \left\{ \left(\frac{\partial\phi_0}{\partial r}\right)_a^2 + \left(\frac{1}{r}\frac{\partial\phi_0}{\partial\theta}\right)_a^2 + 2W\left[\left(\frac{\partial\phi_0}{\partial r}\right)\left(\frac{\partial\phi_1}{\partial r}\right) + \left(\frac{1}{r}\frac{\partial\phi_0}{\partial\theta}\right)\left(\frac{1}{r}\frac{\partial\phi_1}{\partial\theta}\right)\right]_a \right\} + O(W^2), \tag{4}$$

where P_0 is the gas-flow stagnation pressure. This is, upon substitution of the explicit form of the potential to first order,

$$\left.\begin{aligned} \left(\frac{\partial\phi_0}{\partial r}\right)_a &\simeq 2UWf_1(\theta)\cos\theta, \quad \left(\frac{1}{r}\frac{\partial\phi_0}{\partial\theta}\right)_a \simeq 2U[1-Wf_1(\theta)]\sin\theta, \\ p_a(\theta) &\simeq P_0 - 2\rho_g U^2 \sin\theta\left\{[1-2Wf_1(\theta)]\sin\theta + \frac{W}{U}\left(\frac{1}{r}\frac{\partial\phi_1}{\partial\theta}\right)_a\right\}. \end{aligned}\right\} \tag{5}$$

Substitution in the expression for the curvature in polar co-ordinates leads to

$$\frac{1}{R} \simeq \frac{1}{a_0}[1-Wf_1(\theta)-Wf_1''(\theta)]. \tag{6}$$

Inserting (5) and (6) into (1) and rearranging, we obtain

$$Wf_1''(\theta)+Wf_1(\theta) = 1-\frac{E-P_0}{\delta/a_0}-2W\sin^2\theta. \tag{7}$$

A particular solution of (7) is

$$Wf_1(\theta) = 1-\frac{E-P_0}{\delta/a_0}-W(1+\tfrac{1}{3}\cos 2\theta), \tag{8}$$

and the general solution vanishes identically owing to the requirement of symmetry around $\theta = 0, \frac{1}{2}\pi$.

The value of the constant E is obtained by applying the definition of a_0 as the equivalent radius of the cylinder. The cylinder cross-section area is given by:

$$S = \frac{1}{2}\int_0^{2\pi} a^2 d\theta = \pi a_0^2. \tag{9}$$

Substituting (2) leads to

$$S \simeq \tfrac{1}{2}a_0^2\int_0^{2\pi}[1+Wf_1(\theta)]^2 d\theta \simeq \pi a_0^2 + Wa_0^2\int_0^{2\pi} f_1(\theta)\,d\theta, \tag{10}$$

so that

$$\int_0^{2\pi} f_1(\theta)\,d\theta = 0. \tag{11}$$

Substitution of (8) gives, after integration,

$$E = \frac{\delta}{a_0}(1-W)+P_0, \tag{12}$$

and thus the cross section shape is given, to first order, by

$$a^{(1)}(\theta) = a_0(1-\tfrac{1}{3}W\cos 2\theta). \tag{13}$$

We now find $\phi_1(r,\theta)$, the first perturbation of the gas-flow velocity potential. The kinematic boundary condition on the cylinder boundary is $(\nabla\phi\,.\,\vec{\mathbf{n}})_a = 0$, where $\vec{\mathbf{n}}$ is the local normal to the interface, in polar co-ordinates.

Substitution of (3) and (13) leads to

$$\left(\frac{\partial\phi_1}{\partial\theta}\right)_{a_0} = U(\tfrac{1}{3}\cos\theta - \cos 3\theta). \tag{14}$$

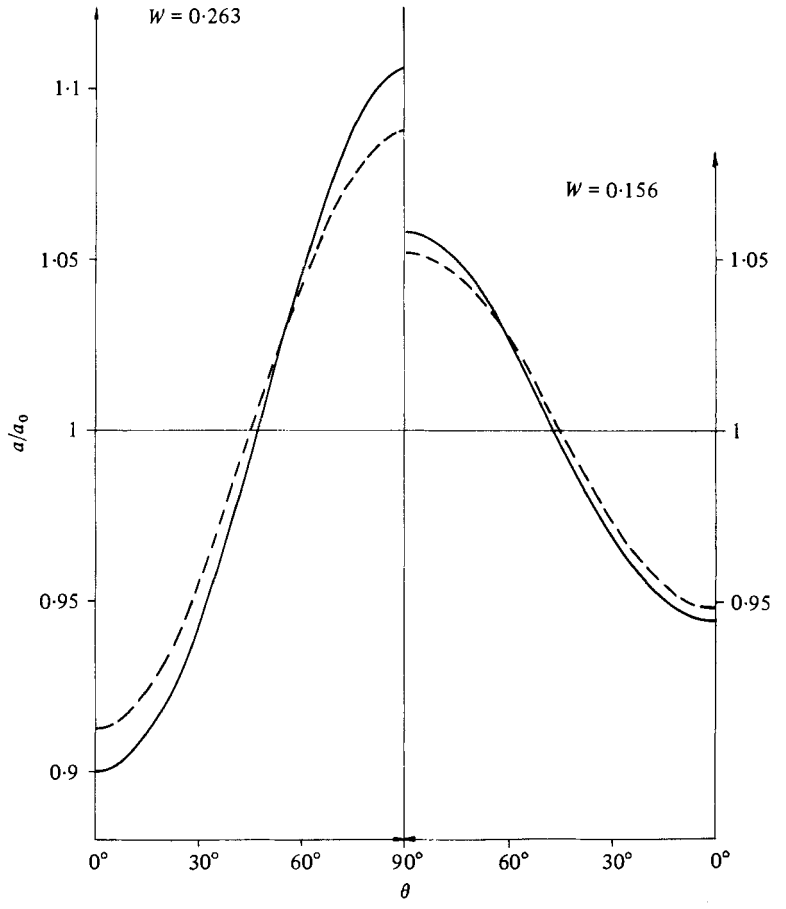

FIGURE 3. Calculated deviations from circularity of the cross-section, comparing calculations by means of the first-order solution (13) (– – –) and the second-order solution (16) (——).

We now seek a ϕ_1 that satisfies Laplace's equation $\nabla^2\phi_1 = 0$ in the region $r \geqslant a(\theta)$, and the boundary conditions (14) and $\phi_1 \to 0$ as $r \to \infty$. By separation of variables and applying the condition of symmetry around $\theta = 0$ and (14), this is

$$\phi_1 = -\tfrac{1}{3}Ua_0\left[\frac{a_0}{r}\cos\theta - \left(\frac{a_0}{r}\right)^3\cos 3\theta\right]. \tag{15}$$

A second-order solution is now constructed in a similar fashion, by retaining terms up to $O(W^2)$ and applying the first-order solutions (13) and (15). The cross-section shape is

$$a^{(2)}(\theta) \simeq a_0[1 - \tfrac{1}{3}W\cos 2\theta - \tfrac{1}{180}W^2(5 + 40\cos 2\theta - 14\cos 4\theta)], \tag{16}$$

and the perturbation potential is

$$\phi_2 = -\tfrac{1}{3}Ua_0\left[\frac{a_0}{r}\cos\theta - \frac{59}{60}\left(\frac{a_0}{r}\right)^3\cos 3\theta + \frac{13}{20}\left(\frac{a_0}{r}\right)^5\cos 5\theta\right]. \tag{17}$$

Typical cross-section shapes appear in figure 3, which shows $a^{(1)}(\theta)/a_0, a^{(2)}(\theta)/a_0$ in the range $0 \leqslant \theta \leqslant \frac{1}{2}\pi$ for values of $W = 0{\cdot}156, 0{\cdot}263$. (The description in the first quadrant is sufficient, since the solution is symmetric about $\theta = 0, \frac{1}{2}\pi$.)

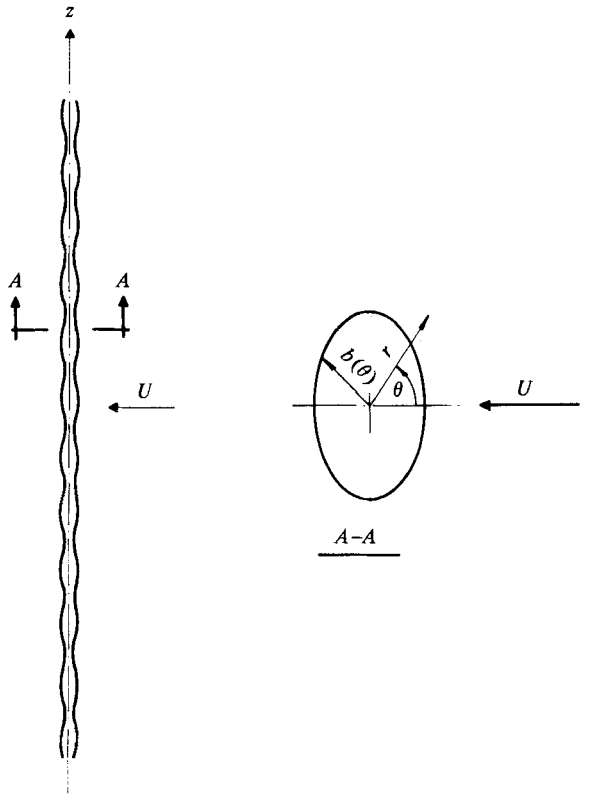

FIGURE 4. Co-ordinates and form of diverging perturbations.

The fineness ratio h, defined as $h \equiv a(0)/a(\frac{1}{2}\pi)$, gives a convenient measure of the 'total' distortion of the cross-section. From (13) and (16) we see that

$$h^{(1)} = \frac{a^{(1)}(0)}{a^{(1)}(\frac{1}{2}\pi)} = 1 - \tfrac{2}{3}W, \quad h^{(2)} = \frac{a^{(2)}(0)}{a^{(2)}(\frac{1}{2}\pi)} = 1 - \tfrac{2}{3}W - \tfrac{2}{9}W^2. \tag{18}$$

Various tests on the range of Weber numbers for which the first and second approximations to the shape and pressure are applicable have been made (Frankel 1980). These include the relative changes in calculated maximal distortion, and in the average distortion, as well as the fineness ratio above. These lead to the expected result, that $a^{(1)}(\theta)$ is a good description for $W < 0{\cdot}3$, while $a^{(2)}(\theta)$ probably is reliable to $W \simeq 0{\cdot}5$.

4. Stability analysis

The stability of the liquid cylinder is analysed by assuming small perturbations of the equilibrium state established in § 3. Let the form of the perturbed cylinder be given by

$$b = a(\theta)(1+\eta), \tag{19}$$

where $r = a(\theta)$ is the equilibrium cross-section shape (16) and η is a small perturbation of the general form $\eta = \eta_0(\theta)\, e^{\beta t + ikz}$. β is the growth rate, k the wavenumber, t is the

time and r, θ, z the cylindrical co-ordinate system (see figure 4). We represent the gas velocity potential Φ by

$$\Phi = \phi(r, \theta) + \hat{\chi}(r, \theta, z, t), \tag{20}$$

where ϕ is, from (3), (15) and (17),

$$\phi = -Ua_0\left\{\left(\frac{r}{a_0}+\frac{a_0}{r}\right)\cos\theta + \tfrac{1}{3}W\left[\frac{a_0}{r}\cos\theta - \left(\frac{a_0}{r}\right)^3\cos 3\theta\right] + \tfrac{1}{3}W^2\left[\frac{a_0}{r}\cos\theta - \frac{59}{60}\left(\frac{a_0}{r}\right)^3\cos 3\theta + \frac{13}{20}\left(\frac{a_0}{r}\right)^5\cos 5\theta\right]\right\}, \tag{21}$$

and $\hat{\chi}$ is the perturbation potential, which is presumably $O(\eta)$.

The kinematic boundary condition on the perturbed gas–liquid interface is:

$$(\hat{v}_r)_b = \frac{Db}{Dt} = \frac{\partial b}{\partial t} + \frac{(\hat{v}_\theta)_b}{b}\frac{\partial b}{\partial \theta} + (\hat{v}_z)_b\frac{\partial b}{\partial z}, \tag{22}$$

where $\hat{v}_r$, $\hat{v}_\theta$, $\hat{v}_z$ are the velocity components.

Substituting (16) and (19)–(21), neglecting terms $O(\eta^2)$ and subtracting the kinematic boundary condition in the equilibrium state

$$\left(\frac{\partial \phi}{\partial r}\right)_a - \frac{1}{a}\frac{da}{d\theta}\left(\frac{1}{r}\frac{\partial \phi}{\partial \theta}\right)_a = 0, \tag{23}$$

we obtain

$$\left(\frac{\partial \hat{\chi}}{\partial r}\right)_b - \tfrac{2}{3}W\sin 2\theta\left(\frac{1}{r}\frac{\partial \hat{\chi}}{\partial \theta}\right)_b = U\eta[\tau + 2\cos\theta + \tfrac{1}{3}W(2\cos\theta - \tau\cos 2\theta - 8\cos 3\theta)] + 2U(\sin\theta - \tfrac{1}{3}W\sin 3\theta)\frac{\partial \eta}{\partial \theta}, \tag{24}$$

where $\tau = \beta a_0/U$.

In order to find a $\hat{\chi}$ that satisfies Laplace's equation $\nabla^2\hat{\chi} = 0$ in the region $r \geqslant b$ and the boundary condition (24), we represent it as the sum $\hat{\chi} = \hat{\chi}_{\mathrm{I}} + \hat{\chi}_{\mathrm{II}}$, where $\hat{\chi}_{\mathrm{I}}$ satisfies the boundary condition

$$\left(\frac{\partial \hat{\chi}_{\mathrm{I}}}{\partial r}\right)_{a_0} = U\eta(\tau + 2\cos\theta) + 2U\frac{\partial \eta}{\partial \theta}\sin\theta, \tag{25}$$

and $\hat{\chi}_{\mathrm{II}}/\hat{\chi}_{\mathrm{I}} = O(W)$. (The appropriate boundary condition for $\hat{\chi}_{\mathrm{II}}$ may be constructed easily by substituting the expression found for $\hat{\chi}_{\mathrm{I}}$ in (24).)

By separation of variables and substitution into the boundary condition together with the series expression for $\eta_0(\theta)$,

$$\eta_0(\theta) = \eta_0\left(A_0 + \sum_{m=1}^{\infty} A_m\cos m\theta + B_m\sin m\theta\right), \tag{26}$$

neglecting higher-order terms we arrive at

$$\hat{\chi} = Ua_0\eta_0 e^{\beta t + ikz}\left\{A_0\left[\tau\frac{K_0(kr)}{\xi K_0'(\xi)} + 2\frac{K_1(kr)}{\xi K_1'(\xi)}\cos\theta\right] + \sum_{m=1}^{\infty} A_m\left[-(m-1)\frac{K_{m-1}(kr)}{\xi K_{m-1}'(\xi)}\cos(m-1)\theta + \tau\frac{K_m(kr)}{\xi K_m'(\xi)}\cos m\theta + (m+1)\frac{K_{m+1}(kr)}{\xi K_{m+1}'(\xi)}\cos(m+1)\theta\right] + B_m\left[-(m-1)\frac{K_{m-1}(kr)}{\xi K_{m-1}'(\xi)}\sin(m-1)\theta + \tau\frac{K_m(kr)}{\xi K_m'(\xi)}\sin m\theta + (m+1)\frac{K_{m+1}(kr)}{\xi K_{m+1}'(\xi)}\sin(m+1)\theta\right] + O(W)\right\}, \tag{27}$$

which satisfies the requirement $\hat{\chi} \to 0$ as $r \to \infty$.

$\xi = ka_0$ is the non-dimensional wavenumber and K_n is the modified Bessel function of the second kind and order n.

In addition to the set of assumptions underlying the solution of the equilibrium state, we further neglect the influence of liquid viscosity on the stability. According to Weber (1931) this additional assumption is justified provided that $\mu_1(2\rho_1\delta a_0)^{-\frac{1}{2}} \ll 1$, where μ_1 is the liquid viscosity and ρ_1 is the liquid density. Most practical cases of spraying or industrial processes satisfy this condition, so that this assumption does not add any new restrictions on applicability. Thus one can write a potential for the liquid phase. The perturbation potential within the liquid, χ, should satisfy the kinematic boundary condition (analogous to (24))

$$\left(\frac{\partial\chi}{\partial r}\right)_b - \tfrac{2}{3}W\sin 2\theta\left(\frac{1}{r}\frac{\partial\chi}{\partial\theta}\right)_b = U\tau(1-\tfrac{1}{3}W\cos 2\theta)\,\eta. \tag{28}$$

By a similar procedure to that described above ((24)–(27)), and using appropriate recurrence relations, we find a χ that satisfies Laplace's equation $\nabla^2\chi = 0$ in the region $0 \leqslant r \leqslant b$ and is bounded for $r = 0$.

The gas-pressure distribution $\hat{P}_b$ on the perturbed interface is given by Bernoulli's law:

$$\hat{P}_b = P_0 - \rho_g\left(\frac{\partial\hat{\chi}}{\partial t} + \tfrac{1}{2}\hat{q}^2\right)_b, \tag{29}$$

where $\hat{q}$ is the local gas speed. $\hat{P}_b$ may be written as a sum $p_a + \hat{p}_b$, where p_a is the gas pressure on the interface in the unperturbed state and $\hat{p}_b$ is the gas-pressure perturbation.

Substituting (16), (19)–(21), (26) and (27) in (29) and subtracting the equation

$$p_a = P_0 - \tfrac{1}{2}\rho_g\left[\left(\frac{\partial\phi}{\partial r}\right)_a^2 + \left(\frac{1}{r}\frac{\partial\phi}{\partial\theta}\right)_a^2\right], \tag{30}$$

that results from the unperturbed state, we obtain an expression for $\hat{p}_b$.

In a similar manner

$$p_b = -\rho_1\left(\frac{\partial\chi}{\partial t}\right)_b, \tag{31}$$

where p_b is the pressure perturbation within the liquid cylinder. (The dynamic-pressure term is omitted since it is $O(\eta^2)$.)

According to (19) the equation of the interface may be written as

$$H(r,\theta,z) = r - a(\theta)\,(1+\eta) = 0,$$

and thus

$$\frac{1}{R_1} + \frac{1}{R_2} = \operatorname{div}\frac{\nabla H}{|\nabla H|},$$

where R_1, R_2 are the principal radii of curvature.

The equilibrium condition on the perturbed gas liquid interface is:

$$p_b - \hat{p}_b = \delta\left[\left(\frac{1}{R_1} + \frac{1}{R_2}\right) - \frac{1}{R}\right]. \tag{32}$$

By substitution of the explicit forms of (29) and (31), and the radii of curvature, and neglecting terms $O(W^2\eta)$ relative to $O(W\eta)$, (32) can be written as a sum of orthogonal disturbance modes.

The orthogonality properties of the trigonometric functions result in the requirement that each of the coefficients of $\cos l\theta (l = 0, 1, \ldots)$ or $\sin l\theta (l = 1, 2, \ldots)$ in (32) vanish separately. This requirement yields a set of equations for the coefficients A_m and another very similar set of equations for the coefficients B_m.†

For $l = 0$

$$(a_{00} - \bar{\tau}^2) A_0 + \gamma \bar{\tau} a_{01} A_1 + W(a_{02} + \alpha_{02}\bar{\tau}^2) A_2 = 0. \tag{33}$$

For $l = 1$

$$\gamma \bar{\tau} a_{10} A_0 + [a_{11} - \bar{\tau}^2(1 + W\alpha_{11})] A_1 + \gamma \bar{\tau} \alpha_{12} A_2 + W(a_{13} + \alpha_{13}\bar{\tau}^2) A_3 = 0. \tag{34}$$

For $l = 2$

$$W(a_{20} + \alpha_{20}\bar{\tau}^2) A_0 + \gamma \bar{\tau} a_{21} A_1 + (a_{22} - \bar{\tau}^2) A_2 + \gamma \bar{\tau} a_{23} A_3 + W(a_{24} + \alpha_{24}\bar{\tau}^2) A_4 = 0. \tag{35}$$

For $l \geqslant 3$

$$W(a_{l,l-2} + \alpha_{l,l-2}\bar{\tau}^2) A_{l-2} + \gamma \bar{\tau} a_{l,l-1} A_{l-1} + (a_{ll} - \bar{\tau}^2) A_l + \gamma \bar{\tau} a_{l,l+1} A_{l+1} + W(a_{l,l+2} + \alpha_{l,l+2}\bar{\tau}^2) A_{l+2} = 0, \tag{36}$$

where

$$\bar{\tau}^2 = W \frac{\rho_1}{\rho_g} \tau^2, \quad \gamma = \left(\frac{\rho_g}{\rho_1} W\right)^{\frac{1}{2}}.$$

Taking the first n rows, excluding the last term in the $(n-1)$th row and the last two terms in the nth row, we arrive at a homogeneous set of n equations in the n unknowns $A_0, A_1, \ldots, A_{n-1}$. This leads to the formulation of the problem of the determination of $\bar{\tau}^2$ as an eigenvalue problem: nontrivial solutions will exist for eigenvalues that fulfil the characteristic equation (37), (p. 403).

When $W \neq 0$ it can be shown by some rather lengthy algebraic manipulation (Frankel 1980) that

$$\bar{\tau}_l^2 = \begin{cases} a_{ll} = \dfrac{\xi I_l'}{I_l}\left\{1 - \xi^2 - l^2 - W\left[2 + (l-1)^2 \dfrac{K_{l-1}}{\xi K_{l-1}'} + (l+1)^2 \dfrac{K_{l+1}}{\xi K_{l+1}'}\right]\right\} \quad (l = 0, 2, 3, \ldots), & (38a) \\ a_{11}(1 - W\alpha_{11}) = -\dfrac{\xi I_1'}{I_1}\left[\xi^2 + W\left(2 + \dfrac{4K_2}{\xi K_2'} - \tfrac{1}{6}\xi^2\right)\right]\left[1 + \tfrac{1}{6}W\left((1 - \xi^2)\dfrac{I_1}{\xi I_1'} + 2 + \dfrac{\xi I_1'}{I_1}\right)\right] \quad (l = 1), & (38b) \end{cases}$$

where I_n, K_n are the modified Bessel functions of argument ξ, when terms $O(W^2)$ or higher are omitted.

If $W = 0$, all the non-diagonal elements are identically zero, and we retrieve

$$\bar{\tau}_l^2 = a_{ll} = \frac{\xi I_l'}{I_l}(1 - \xi^2 - l^2),$$

which is Rayleigh's solution.

The perturbation form (eigenvector) associated with the growth rate (eigenvalue) $\bar{\tau}_l^2$ is approximately

$$\eta_l \simeq \eta_0 e^{\beta t + ikz}[\cos l\theta + O(W)] \quad (l = 0, 1, \ldots), \tag{39}$$

i.e. the components of $\cos k\theta, k \neq l$, in η_l are $O(W)$ or higher.

† The explicit expressions for the coefficients a_{ij}, α_{ij}, further details of the series form of (32) and previous steps may be obtained directly from the authors.

$$
\begin{vmatrix}
1-\dfrac{\bar{\tau}^2}{a_{00}} & \gamma\bar{\tau}\dfrac{a_{01}}{a_{00}} & W\left(\dfrac{a_{02}}{a_{00}}+\alpha_{02}\dfrac{\bar{\tau}^2}{a_{00}}\right) & 0 & 0 & 0 & 0 & \cdots & 0 \\
\gamma\bar{\tau}\dfrac{a_{10}}{a_{11}} & 1-\dfrac{\bar{\tau}^2}{a_{11}}(1+W\alpha_{11}) & \gamma\bar{\tau}\dfrac{a_{12}}{a_{11}} & W\left(\dfrac{a_{13}}{a_{11}}+\alpha_{13}\dfrac{\bar{\tau}^2}{a_{11}}\right) & 0 & 0 & 0 & \cdots & 0 \\
W\left(\dfrac{a_{20}}{a_{22}}+\alpha_{20}\dfrac{\bar{\tau}^2}{a_{22}}\right) & \gamma\bar{\tau}\dfrac{a_{21}}{a_{22}} & 1-\dfrac{\bar{\tau}^2}{a_{22}} & \gamma\bar{\tau}\dfrac{a_{23}}{a_{22}} & W\left(\dfrac{a_{24}}{a_{22}}+\alpha_{24}\dfrac{\bar{\tau}^2}{a_{22}}\right) & 0 & 0 & \cdots & 0 \\
0 & — & — & — & — & — & 0 & \cdots & 0 \\
0 & 0 & — & — & — & — & — & \cdots & 0 \\
\vdots & \vdots & \vdots & \vdots & \vdots & \vdots & \vdots & & \cdots
\end{vmatrix} = 0. \tag{37}
$$

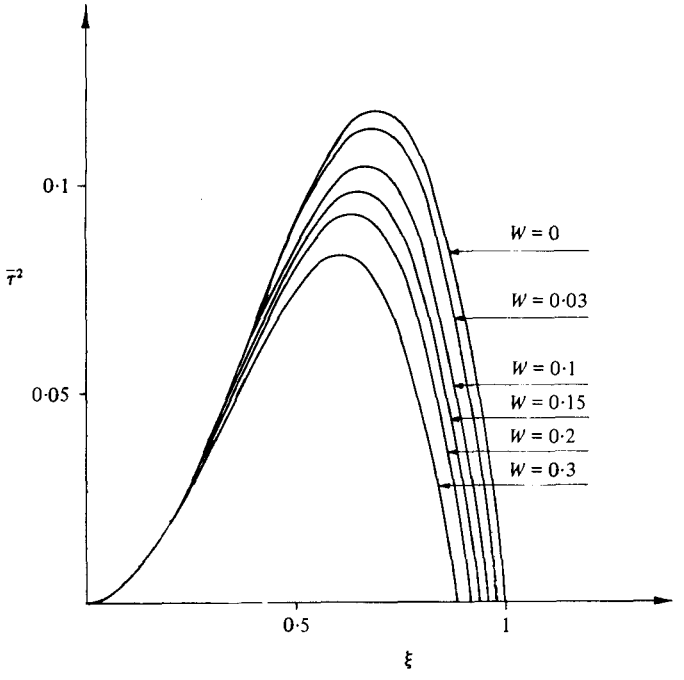

FIGURE 5 Square of non-dimensional temporal growth rate of diverging perturbations *vs.* non-dimensional wavenumber of perturbation. Parameter is Weber number.

The set of equations for B_m, the coefficients of the sine functions in (32), is very similar to the set for the coefficients A_m. They yield the same eigenvalues $\bar{\tau}_l^2$, with the only difference being that for $l = 1$

$$\bar{\tau}_1^2 = -\frac{\xi I_1'}{I_1}\left[\xi^2 + W\left(2 + \frac{4K_2}{\xi K_2'} + \tfrac{1}{6}\xi^2\right)\right]\left\{1 - \tfrac{1}{6}W\left[(1-\xi^2)\frac{I_1}{\xi I_1'} + 2 + \frac{\xi I_1'}{I_1}\right]\right\}. \tag{40}$$

The eigenvectors are now

$$\eta_l \simeq \eta_0 e^{\beta t + ikz}[\sin l\theta + O(W)] \quad (l = 1, 2, \ldots). \tag{41}$$

For any perturbation to lead to instability, the square of its non-dimensional growth rate $\bar{\tau}_l^2$ as given by (38), (40) must be positive.

For $l = 2, 3, \ldots$, since $\xi I_l'/I_l > 0$ for all $\xi \geqslant 0$, the sign of $\bar{\tau}_l^2$ is determined by the expression in brackets on the right-hand side of (38*a*). For all $\xi \geqslant 0$ $K_l/\xi K_l'$ is negative, monotonically increasing, and tends asymptotically to zero for $\xi \to \infty$. Thus the highest value of $\bar{\tau}_l^2$ is for $\xi \to 0$: $\bar{\tau}_l^2 = -l(l-1)(l+1-2W)$. For these perturbations to lead to instabilities: $W \geqslant \frac{1}{2}(l+1)$. We can conclude that these forms are not involved in the break-up process of the liquid cylinder in the region of low Weber numbers ($W < 1$) we are dealing with.

For $l = 1$; the expressions for $\bar{\tau}_1^2$, (38*b*) and (40), lead to the same conclusion, i.e. that these forms are also non-divergent when the Weber number is smaller than unity.

The only perturbation which causes instability is thus the 'varicose' one given by

$$\eta = \eta_0 e^{\beta t + ikz}[1 + O(W)], \tag{42}$$

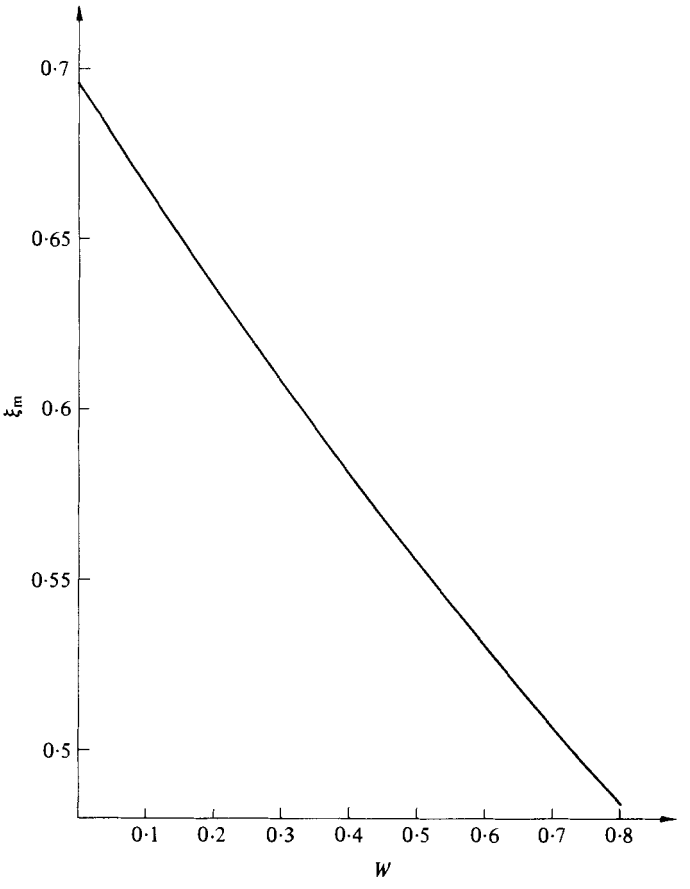

FIGURE 6. Non-dimensional wavenumber of varicose perturbation of maximum growth rate *vs.* Weber number.

for which:

$$\bar{\tau}_0^2 = \frac{\xi I_0'}{I_0}\left[1-\xi^2-2W\left(1+\frac{K_1}{\xi K_1'}\right)\right]. \tag{43}$$

Figure 5 shows the dependence of $\bar{\tau}_0^2$ on the non-dimensional wavenumber for several values of W. Increasing the Weber number is seen to decrease the growth rate of the varicose perturbations. The maximal wavenumber for which the perturbations diverge and ξ_m, the wavenumber of the perturbation which has maximum growth rate are decreased as well.

The variation of ξ_m with W appears in figure 6. ξ_m is seen to decrease nearly linearly with the Weber number up to $W \simeq 0{\cdot}3$.

5. Discussion

The variation of the characteristics of the varicose perturbation with the Weber number as shown in figures 5 and 6 may be accounted for through the identification of the origin of the terms in $\bar{\tau}_0^2$ (equation (43)) that include W. Thus we find that the

perturbation of the pressure distribution in the gas flow includes a term

$$2\rho_g U^2(1+K_1/\xi K_1')$$

due to the varicose perturbation of the liquid cylinder. This appears in the expression for $\bar{\tau}_0^2$ as $-2W(1+K_1/\xi K_1')$.

For all $\xi \geqslant 0, 1+K_1/\xi K_1' > 0$. Thus there is an increase in gas pressure where the cylinder 'swells' ($\eta > 0$) while the gas pressure decreases where the liquid cylinder narrows ($\eta < 0$). Thus a pressure distribution forms that opposes the development of the varicose perturbations; this explains the decrease of the value of $\bar{\tau}_0^2$ with the increase in W. These changes in pressure distribution become physically clear if we visualize the three-dimensional gas flow about the perturbed liquid cylinder.

Once the cylinder has started to distort owing to a varicose perturbation, it becomes 'easier' for the flow to move past the constricted sections, causing higher velocity there, and thus the predicted lower pressure is produced. The pressures are thus higher at the expanded sections and this three-dimensional flow field tends to stabilize the cylinder, causing the reduction in $\bar{\tau}_0^2$.

Furthermore, since $1+K_1/\xi K_1'$ is monotonically increasing there is higher resistance against the divergence of varicose perturbations the higher the value of ξ. Consequently, the limiting wavenumber for divergence and the wavenumber of maximum growth rate are both reduced with increasing the Weber number.

The present linear solution cannot be expected to describe the actual break-up of the cylinder reliably. Nevertheless, it is a commonly accepted assumption that the perturbation of maximum growth rate in the 'linear' range of small perturbations penetrates the 'nonlinear' range and dominates the actual break-up. Thus we expect the liquid cylinder to be destabilized and broken up by the varicose perturbations of wavenumber ξ_m. Assuming that one drop is formed from each segment of one wavelength (neglecting the influence of the satellite droplets, which include up to 4 % of the mass (Bogy 1979)), we obtain by mass conservation

$$\frac{c_0}{a_0} = \left(\frac{3\pi}{2\xi_m}\right)^{\frac{1}{3}}, \tag{44}$$

where c_0 is the drop radius.

As we have noted above, figure 6 shows ξ_m to decrease nearly linearly with W up to $W \simeq 0{\cdot}3$. This dependence may be approximated by

$$\frac{\xi_m}{\xi_{m0}} \cong 1-0{\cdot}43W \quad (0 \leqslant W \leqslant 0{\cdot}3), \tag{45}$$

where $\xi_{m0} = 0{\cdot}697$ is the value of ξ_m for the case $W = 0$ (Rayleigh's solution). Substituting (45) we obtain

$$\frac{c_0}{a_0} \simeq \left(\frac{c_0}{a_0}\right)_0 (1+0{\cdot}14W) \quad (0 \leqslant W \leqslant 0{\cdot}3), \tag{46}$$

where

$$\left(\frac{c_0}{a_0}\right)_0 = \left(\frac{3\pi}{2\xi_{m0}}\right)^{\frac{1}{3}} \simeq 1{\cdot}89$$

is the ratio of the radii for $W = 0$.

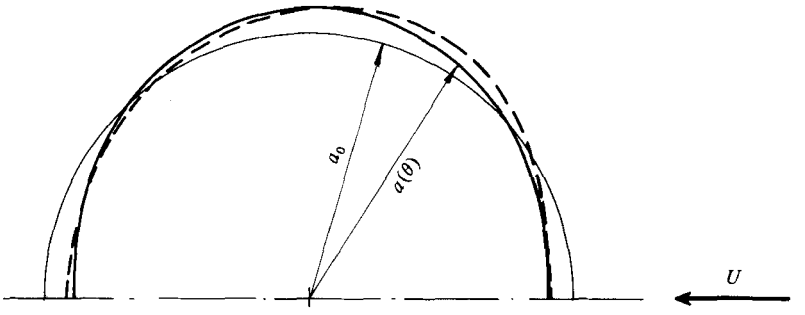

FIGURE 7. Comparison of the calculated equilibrium cross-section with (broken line) and without (thick full line) corrections for flow separation. a_0 is the circular cross-section obtained when $U = 0$ ($W = 0$).

Thus the cross flow is seen to increase the wavelength of maximum instability and, through it, the size of droplets produced after the instability leads to break-up of the cylinder.

Appendix. On the influence of flow separation on the cross-sectional shape

A rough estimate of the influence of flow separation on the equilibrium shape can be obtained by the following modification of the solution in § 3.

Let θ_s be the angle at which the gas flow separates. We assume that in the region $0 \leqslant \theta \leqslant \theta_s$, the gas flow is described by potential flow while in the region $\theta_s \leqslant \theta \leqslant \pi$ there is a uniform pressure, assumed to be the pressure p_∞ of the undisturbed gas flow far upstream of the liquid cylinder.

In an identical manner to § 3 (equation (8)) the equilibrium condition in the region $0 \leqslant \theta \leqslant \theta_s$ results in

$$Wf_1(\theta) = 1 - \frac{E - P_0}{\delta/a_0} - W(1 + \tfrac{1}{3}\cos 2\theta) + A\cos\theta, \tag{A 1}$$

since there is no symmetry about $\theta = \frac{1}{2}\pi$ in this case.

In the region $\theta_s \leqslant \theta \leqslant \pi$ the equilibrium condition is

$$P_0 - \tfrac{1}{2}\rho_g U^2 + \frac{\delta}{a_s} = E,$$

or

$$\frac{a_0}{a_s} = \tfrac{1}{2}W + \frac{E - P_0}{\delta/a_0}, \tag{A 2}$$

where $r = a_s$ describes the gas liquid interface in the region $\theta_s \leqslant \theta \leqslant \pi$. (Because of the assumption of uniform gas pressure, a_s is, of course, constant.)

To obtain a continuous and smooth boundary, we impose the conditions:

$$a(\theta_s) = a_s, \quad \left(\frac{da}{d\theta}\right)_{\theta_s} = 0. \tag{A 3}$$

Combining (A 1)–(A 3) and ignoring the trivial solutions $\theta_s = 0, \pi$, we obtain

$$\cos\theta_s = \pm\tfrac{1}{2}. \tag{A 4}$$

Laminar separation from a solid cylinder occurs at approximately $\theta = 0{\cdot}6\pi$, so that θ_s should be in the region $\frac{1}{2}\pi < \theta_s < \pi$. Thus we choose the negative solution of (A 4), resulting in $\theta_s = \frac{2}{3}\pi$ and

$$A = -\tfrac{2}{3}W. \tag{A 5}$$

The gas pressure is discontinuous at θ_s. This inevitable discontinuity results from the rather crude approximation involved in this modified solution.

The value of E may be determined as before. Here the cross section S is given by

$$S = \int_0^{\theta_s} a^2 d\theta + (\pi - \theta_s)\, a_s^2 = \pi a_0^2.$$

Substitution of (A 1), (A 3) and (A 4) and integration leads to

$$\frac{a(\theta)}{a_0} = \begin{cases} 1 - \left(\dfrac{1}{6} - \dfrac{3^{\frac{1}{2}}}{4\pi}\right) W - \tfrac{2}{3}W\cos\theta - \tfrac{1}{3}W\cos 2\theta & (0 \leqslant \theta \leqslant \tfrac{2}{3}\pi), \\ 1 + \left(\dfrac{1}{3} + \dfrac{3^{\frac{1}{2}}}{4\pi}\right) W & (\tfrac{2}{3}\pi \leqslant \theta \leqslant \pi). \end{cases} \tag{A 6}$$

The equilibrium shape (A 6) for $W = 0{\cdot}3$ appears in figure 7, together with the first-order shape $a^{(1)}$ obtained from (13), and a_0. It is seen that the flow separation causes only minor changes in section shape and fineness ratio when compared with the distortion from the circular shape.

REFERENCES

Anno, J. N. 1977 *The Mechanics of Liquid Jets.* Lexington.

Bogy, D. B. 1979 *Ann. Rev. Fluid Mech.* **11**, 207.

Brodkey, R. S. 1967 *The Phenomena of Fluid Motions.* Addison-Wesley.

Clark, E. J. & Dombrowski, N. 1972 *Proc. R. Soc. Lond.* A **329**, 467.

Crapper, G. D., Dombrowski, N., Jepson, W. P. & Pyott, G. A. D. 1975 *J. Fluid Mech.* **57**, 671.

Crapper, G. D., Dombrowski, N. & Pyott, G. A. D. 1975 *Proc. R. Soc. Lond.* A **342**, 209.

Dombrowski, N., Hasson, D. & Ward, D. E. 1960 *Chem. Engng Sci.* **12**, 35.

Dombrowski, N. & Hooper, P. C. 1962 *Chem. Engng Sci.* **17**, 291.

Dombrowski, N. & Johns, W. R. 1963 *Chem. Engng Sci.* **18**, 203.

Frankel, I. 1980 Investigation of aerodynamic instabilities leading to atomization of jets, M.Sc. thesis, Technion.

Fraser, R. P., Eisenklam, P., Dombrowski, N. & Hasson, D. 1962 *A.I.Ch.E. J.* **8**, 672.

Hagerty, W. W. & Shea, J. F. 1955 *J. Appl. Mech.* **22**, 509.

LeClair, B. P., Hamielec, A. E., Pruppacher, H. R. & Hall, W. D. 1972 *J. Atmos. Sci.* **29**, 728.

Levich, V. G. 1962 *Physicochemical Hydrodynamics.* Prentice-Hall.

Pruppacher, H. R. & Pitter, R. L. 1971 *J. Atmos. Sci.* **28**, 86.

Rayleigh, Lord 1894 *The Theory of Sound*, 2nd edn. Reprinted 1945 by Dover.

SQUIRE, H. B. 1953 *Brit. J. Appl. Phys.* **4**, 167.
STERLING, A. M. & SLEICHER, C. A. 1975 *J. Fluid Mech.* **68**, 477.
TANASAWA, Y., SASAKI, S. & NAGAI, N. 1957 *Techn. Rep. Tohoku Univ.* **22**, 73.
WEBER, C. 1931 *Z. Angew. Math. Mech.* **11**, 136.
WEIHS, D. 1978 *J. Fluid Mech.* **87**, 289.